Theoretical study of the electronic structure, chemical bonding and optical properties of $KNbO_3$ in the paraelectric cubic phase

2003 J. Phys.: Condens. Matter 15 5945

(http://iopscience.iop.org/0953-8984/15/35/304)

INSTITUTE OF PHYSICS PUBLISHING JOURNAL OF PHYSICS: CONDENSED MATTER

J. Phys.: Condens. Matter **15** (2003) 5945–5958 PII: S0953-8984(03)64530-3

Theoretical study of the electronic structure, chemical bonding and optical properties of $KNbO_3$ in the paraelectric cubic phase

C M I Okoye[1]

Department of Physics and Astronomy, University of Nigeria, Nsukka, Nigeria

E-mail: okoyecmi@yahoo.com

Received 4 June 2003, in final form 28 July 2003
Published 22 August 2003
Online at stacks.iop.org/JPhysCM/15/5945

Abstract

The electronic energy band structure, density of states (DOS) and charge density contour of $KNbO_3$ in the paraelectric cubic phase have been studied using the full-potential linearized augmented plane wave method within the generalized gradient approximation for exchange and correlation. The band structure shows an indirect (R–Γ) band gap. From the DOS analysis as well as charge density studies, we find that the bonding between K and NbO_3 is mainly ionic while that between Nb and O is covalent. We have also reported results on the pressure variation of the energy gap of this compound and found that the band gap increases with increasing pressure. In order to understand the optical properties of the perovskite, the real and imaginary parts of the dielectric function, reflectivity, absorption coefficient, optical conductivity, electron energy-loss function, refractive index and extinction coefficient were calculated. The general profiles of the optical spectra were analysed and origins of the structures discussed.

1. Introduction

Potassium niobate ($KNbO_3$) is one of the most extensively studied compounds of the perovskite class of ferroelectric materials. The perovskite structure is adopted by numerous compounds with ABX_3 stoichiometry, where A and B are cations and X represents anions such as those of oxygen, nitrogen and fluorine [1–4]. The perfect perovskite has full cubic symmetry. The A and B cations are arranged on a simple cubic lattice and the X ions lie on the face centres nearest the (usually transition metal) B cations. The perovskites have been studied extensively because of their rich display of a variety of structural phase transitions [3].

[1] Regular associate of the Abdus Salam ICTP, Trieste, Italy.

0953-8984/03/355945+14$30.00

Potassium niobate, for instance, crystallizes in the simple cubic paraelectric perovskite phase at high temperatures (>710 K). When cooled, it undergoes three ferroelectric phase transitions (at lower temperatures) resulting in a series of distorted perovskite structures, namely, the tetragonal phase, the orthorhombic phase and the ground state rhombohedral phase [4, 5]. Potassium niobate is a perovskite ferroelectric material which is important in a variety of applications in optical technology involving holographic storage, optical data processing, phase conjugation [6], nonvolatile ferroelectric memories, dielectrics for microelectronics and wireless communication [7]. In addition, $KNbO_3$ is a very interesting nonlinear optical (NLO) material because of its high NLO coefficients [8, 9].

In order to fully take advantage of the properties of $KNbO_3$ in the fabrication of optical devices, a theoretical investigation of the electronic structure as well as the optical properties is necessary. Most of the previous theoretical studies have concentrated on the ferroelectricity and/or structural instability [5, 10–13] as well as electronic structure [14–17]. However, only a few first-principles calculations exist in the case of $KNbO_3$ [18, 19]. First-principles calculations offer one of the most powerful tools for carrying out theoretical studies of structural, electronic and optical properties of ferroelectrics [20–26] and other materials [27, 28]. In view of this, we shall employ one such first-principles method in this study in order to elucidate the electronic and optical properties of the material.

The optical properties of the ground state orthorhombic phase of $KNbO_3$ have been studied experimentally [29–31]. Theoretical studies [32–37] have been performed on both the orthorhombic and cubic phases of potassium niobate. In this work, we report the results of a systematic theoretical study based on first-principles calculations of the structural, electronic and optical properties of the paraelectric cubic $KNbO_3$ using full-potential linearized augmented plane wave (FP-LAPW) method [38] with the Perdew–Burke–Ernzerhof (PBE) [39] generalized gradient approximation (GGA) for the exchange and correlation term. In addition, we shall assume that $KNbO_3$ has the ideal cubic perovskite structure, neglecting the slight non-cubic distortions in the crystal structure of $KNbO_3$ below 700 K [40]. The calculations are performed at the experimental lattice constant (extrapolated to zero temperature) $a = 3.996$ Å [41].

The paper is organized as follows. In section 2, we give a brief description of the method of calculation of the ground state and optical properties. The results of the present calculations as well as the discussions are given in section 3 while conclusions are presented in section 4.

2. Method of calculation

The self-consistent calculations for the paraelectric cubic phase of $KNbO_3$ were performed using the nonscalar-relativistic FP-LAPW method [38], within the framework of the density functional theory, at the experimental lattice constant, to allow for ease of comparison. The paraelectric cubic phase of $KNbO_3$ has the ideal cubic $Pm3m$ perovskite structure. The cubic unit cell contains one molecule with the K sitting at the origin $(0, 0, 0)a$, the Nb at the body centre $(0.5, 0.5, 0.5)a$ and the three oxygen atoms at the three face centres $(0.5, 0.5, 0.0)a$, $(0.0, 0.5, 0.5)a$ and $(0.5, 0.0, 0.5)a$, where a is the lattice constant. In the FP-LAPW method [38, 42], the unit cell is divided into two parts: non-overlapping atomic spheres (centred at atomic sites) and an interstitial region. Within these spheres, the potential is expanded in the form

$$V(r) = \sum_{lm} V_{lm}(r) Y_{lm}(\hat{r}) \tag{1}$$

and, outside the sphere,

$$V(r) = \sum_{K} V_K \mathrm{e}^{\mathrm{i}Kr} \tag{2}$$

where the $Y_{lm}(\hat{r})$ are spherical harmonics. The charge density is also expanded analogously. In the following calculations, we have distinguished the K ($1s^2 2s^2 2p^6 3s^2 3p^6$), Nb ($1s^2 2s^2 2p^6 3s^2 3p^6 3d^{10} 4s^2 4p^6$) and O ($1s^2$) inner-shell electrons from the valence electrons of K ($4s^1$), Nb ($4d^3 5s^2$) and O ($2s^2 2p^4$) shells. The sphere radii used in the calculations for K, Nb and O are 1.6, 2.0 and 1.5 au respectively. In this method of calculation, there are no shape approximations to the charge density or potential; hence the procedure is referred to as the 'full-potential' method. The calculations are based on the GGA to the density functional theory [43, 44] with the exchange–correlation potential parametrized according to the scheme of the PBE GGA [39]. Well converged solutions were obtained for $R_{\mathrm{MT}} K_{\max} = 8$; R_{MT} is the smallest of all atomic sphere radii and $K_{\max}$ is the plane wave cut-off. This gives a well converged basis set consisting of 563 plane waves per k-point in the cubic phase. The number of mesh points in the Brillouin zone is 729 and the division of the reciprocal lattice vectors (intervals) is into $9 \times 9 \times 9$ meshes generating 35 k-points in the irreducible wedge.

The pressure dependence of the energy gap for $KNbO_3$ was calculated using the equation [45, 46]

$$\left(\frac{\partial E_{\mathrm{g}}}{\partial P}\right)_T = \left(\frac{\partial E_{\mathrm{g}}}{\partial V}\right)_T \left(\frac{\partial V}{\partial P}\right)_T = -\frac{V_0}{B_0}\left(\frac{\partial E_{\mathrm{g}}}{\partial V}\right)_T. \tag{3}$$

The value of $(\partial E_{\mathrm{g}}/\partial V)_T$ was obtained directly from the energy gap versus volume calculations, and the value of $(\partial V/\partial P)_T$ was obtained from the compressibility relationship:

$$k = \frac{1}{B_0} = -\frac{1}{V_0}\left(\frac{\partial V}{\partial P}\right)_T \tag{4}$$

where V_0 is the equilibrium volume and B_0 is the bulk modulus at the equilibrium volume.

The linear response of the system to an external electromagnetic field with a small wavevector is measured through the complex dielectric function $\varepsilon(\omega)$. Therefore, in order to calculate the optical properties, a dense mesh of uniformly distributed k-points is required. The Brillouin zone integration was performed using the tetrahedron method with 560 k-points in the irreducible part of the Brillouin zone without broadening. The dielectric function is known to describe the optical response of the medium at all photon energies $E = \hbar\omega$. The interband contribution to the imaginary part of the dielectric function $\varepsilon(\omega)$ is calculated by summing transitions from occupied to unoccupied states (with fixed $\boldsymbol{k}$) over the Brillouin zone, weighted with the appropriate matrix elements giving the probability for the transition. In this study, the imaginary part of the dielectric function $\varepsilon_2(\omega)$ is given as in [47] by

$$\varepsilon_2(\omega) = \left(\frac{4\pi^2 e^2}{m^2\omega^2}\right) \sum_{i,j} \int \langle i|M|j\rangle^2 f_i(1 - f_j)\delta(E_f - E_i - \omega)\,\mathrm{d}^3k, \tag{5}$$

where M is the dipole matrix, i and j are the initial and final states respectively, f_i is the Fermi distribution function for the ith state and E_i is the energy of electron in the ith state. The real part ($\varepsilon_1(\omega)$) of the dielectric function can be extracted from the imaginary part using the Kramers–Kronig relation in the form [48, 49]

$$\varepsilon_1(\omega) = 1 + \frac{2}{\pi}\,\mathrm{P}\int_0^\infty \frac{\omega'\varepsilon_2(\omega')\,\mathrm{d}\omega'}{(\omega'^2 - \omega^2)}, \tag{6}$$

where P stands for the principal value of the integral.

The knowledge of both the real and imaginary parts of the dielectric tensor allows the calculation of important optical functions. In this paper, we also present and analyse some optical functions such as the reflectivity, the absorption coefficient, the real part of the optical conductivity, the electron energy-loss spectrum, the refractive index, as well as the extinction coefficient. The reflectivity spectrum is derived from Fresnel's formula for normal

incidence assuming an orientation of the crystal surface parallel to the optical axis using the relation [49, 50]

$$R(\omega) = \left| \frac{\varepsilon^{1/2}(\omega) - 1}{\varepsilon^{1/2}(\omega) + 1} \right|^2. \tag{7}$$

We calculate the absorption coefficient, $I(\omega)$, the real part of the optical conductivity, $\mathrm{Re}[\sigma(\omega)]$, and the electron energy-loss function, $-\mathrm{Im}(1/\varepsilon)$, using the following expressions [50]:

$$I(\omega) = \sqrt{2}(\omega)\left(\sqrt{\varepsilon_1(\omega)^2 + \varepsilon_2(\omega)^2} - \varepsilon_1(\omega)\right)^{1/2}, \tag{8}$$

$$\mathrm{Re}[\sigma(\omega)] = \frac{\omega\varepsilon_2}{4\pi}, \tag{9}$$

$$-\mathrm{Im}\left(\frac{1}{\varepsilon}\right) = \frac{\varepsilon_2(\omega)}{\varepsilon_1^2(\omega) + \varepsilon_2^2(\omega)}. \tag{10}$$

Also, the optical functions such as the refractive index, $n(\omega)$, and the extinction coefficient, $k(\omega)$, are calculated in terms of the components of the complex dielectric function as follows [50]:

$$n(\omega) = \left[\frac{\varepsilon_1(\omega)}{2} + \frac{\sqrt{\varepsilon_1(\omega)^2 + \varepsilon_2(\omega)^2}}{2} \right]^{1/2}, \tag{11}$$

$$k(\omega) = \left[\frac{\sqrt{\varepsilon_1(\omega)^2 + \varepsilon_2(\omega)^2}}{2} - \frac{\varepsilon_1(\omega)}{2} \right]^{1/2}. \tag{12}$$

We have calculated the theoretical optical spectra using equations (5)–(12). However, it is well known that the density functional calculations within the local density approximation (LDA) or GGA tend to underestimate the energies of excitation [51]. As a result, the peaks in the optical functions may occur at lower energies. Usually, one approach adopted in solving the problem of density functional theory (DFT) for excitations from the ground state is the quasiparticle GW formalism [52, 53] which is the formal basis for the scissors-operator approximation. It has been shown [54–57] that LDA/GGA combined with the scissors-operator approximation describes the optical spectrum rather well. If the k-dependence of the error in the excitation energies is negligible, $\Delta(k) \simeq \Delta$, $\varepsilon_2^{GW}(\hbar\omega)$ can be obtained by shifting $\varepsilon_2^{\mathrm{DFT}}(\hbar\omega)$ along the energy axis [56]:

$$\varepsilon_2^{GW}(\hbar\omega) = \varepsilon_2^{\mathrm{DFT}}(\hbar\omega - \Delta). \tag{13}$$

We therefore estimate the correction to the band gap on the basis of the difference between the calculated GGA band gap and the experimental optical gap [57].

3. Results and discussion

3.1. Structural parameters

The total energy of cubic $KNbO_3$ was calculated at many different volumes around the experimental volume and fitted to the Murnaghan equation of state [58]. This gave an equilibrium lattice constant (a_0) of 4.039 Å which is 1.05% larger than the experimental value. This is within the accuracy range of calculations based on density functional GGA. The bulk modulus (B_0) at the experimental equilibrium volume is 170.94 GPa while the first pressure derivative of the bulk modulus (B') is 4.79. These results compare very well with previous theoretical calculations [59]. The bulk modulus is smaller than the experimental value by about 22%. This apparently large discrepancy may be due to the fact that the theoretical

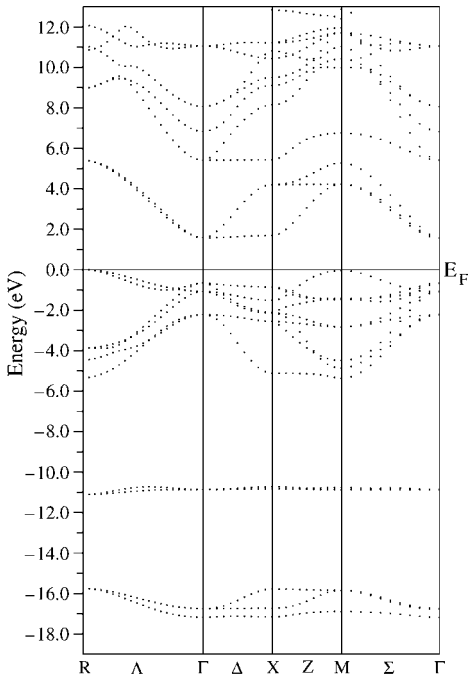

Figure 1. Electronic band structures of cubic $KNbO_3$.

bulk modulus has been calculated in the cubic phase at 0 K while $KNbO_3$ crystal is known to be cubic only in the high temperature range. Furthermore, the experimental bulk modulus may be incorrect due to the uncertainty in the experimentally derived elastic constants from which it was deduced [60].

3.2. Electronic band structure and density of states

The electronic band structure of paraelectric cubic $KNbO_3$ along the symmetry lines of the simple cubic Brillouin zone is shown in figure 1. It is clear that the indirect band gap appears between the topmost valence band at the R point and the bottom of the conduction band at the Γ point. The overall profile of our band structure is qualitatively like the band structure obtained by previous studies [59, 61]. It is observed that the conduction band minimum in going from the Γ point through Δ to the X point always remains nearly flat in agreement with previous studies [33, 62]. The calculated indirect band gap (R–Γ) is 1.58 eV while the smallest direct band gap (Γ_v–Γ_c) is 2.23 eV. These calculated values are smaller than the experimental value of 3.3 eV for the indirect gap [60]. The origin of this discrepancy could be the use of DFT which generally underestimates the band gap in semiconductors and insulators [63].

The bands with the lowest energy in figure 1, lying between −17 and −16.5 eV, correspond, to a very large extent, to O 2s states, while the nearly flat band around −11.0 eV is due to K 3s states. The nine valence bands between −5.5 eV and the Fermi level (zero) are mainly due to oxygen O 2p states hybridized with Nb 4d states. These nine valence bands are split into three triply degenerate levels at the Γ point (Γ_{15}, Γ_{25} and Γ_{15}) separated by energies 1.15 eV (Γ_{15}–Γ_{25}), 0.42 eV (Γ_{25}–Γ_{15}) and 2.23 eV (Γ_{15}–$\Gamma_{25'}$) due to the crystal field and electrostatic interaction between mainly O 2p and Nb 4d orbitals. In the conduction band, the triply (Γ'_{25})

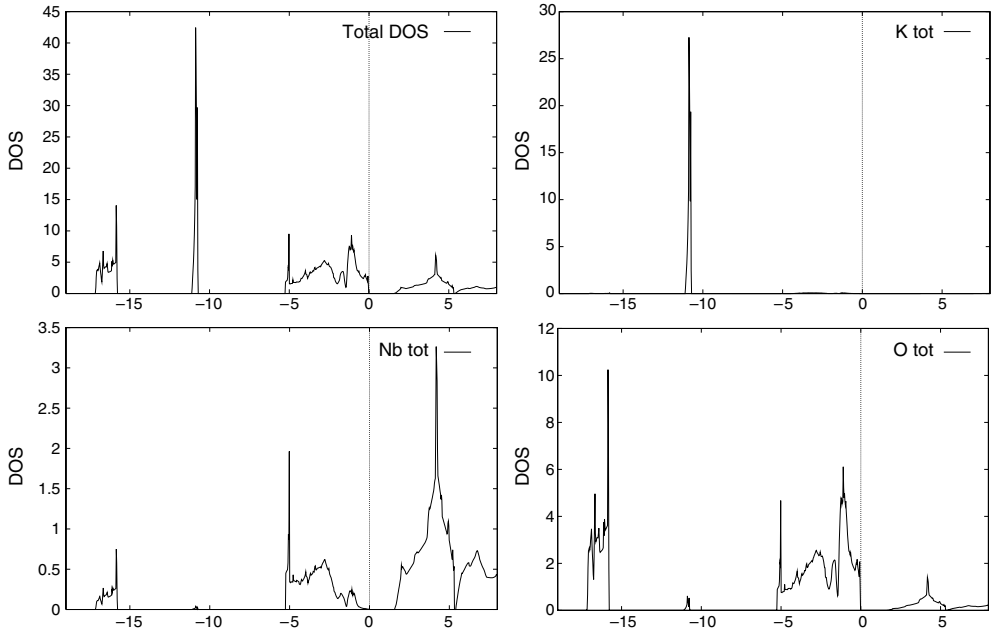

Figure 2. Total and site decomposed DOS for $KNbO_3$.

and doubly (Γ_{12}) degenerate levels represent Nb 4d t_{2g} and Nb 4d e_g orbitals separated by energy ∼3.84 eV. The topmost valence bands are the oxygen $2p_x$, $2p_y$ states while the lowest valence bands are formed by hybridization of Nb 4d e_g and O $2p_z$ states. In the conduction band region, the first conduction band from about 1.6 eV above the Fermi level to ∼5.5 eV arises from predominantly Nb 4d t_{2g} states with a small O 2p mixing. The top bands in the conduction band of figure 1 belong to Nb 4d e_g states.

To further elucidate the nature of the electronic band structure, we have also calculated the total and atomic site projected densities of states (DOS) of ideal cubic $KNbO_3$. These are displayed in figure 2. The results are consistent with those obtained in previous studies [3, 36, 37]. Comparing the total DOS with the angular momentum projected DOS of $KNbO_3$ for Nb 4d and O 2p states displayed in figure 3, it is seen that from −5.5 to 0 eV, even though the DOS for O 2p is higher than that of Nb 3d, they are fairly similar. This shows that some electrons from Nb 4d transform into the valence band and take part in the interaction between Nb and O. This implies that there is hybridization between Nb 4d and O 2p. Conversely, in the conduction band, the DOS of Nb d is much higher than that of O p. This implies that there are few O p electrons which transform into the conduction band and hybridize with Nb d electrons. The DOS of Nb d and O p thus show that the interaction between Nb and O is covalent. On the other hand, the DOS of K 3p shows a peak around −11.0 eV attributed to the flat band around this energy in the band structure. The structures lowest in energy between about −17.5 and −16.0 eV are shown to be of predominantly O 2s character with some mixing of Nb p states. On the whole, our results are in agreement with the LMTO-ASA calculations of Neumann [18] and extended linear augmented plane wave calculations of Krasovskii *et al* [36].

Figure 4 shows the charge density contour in the (110) plane for cubic paraelectric $KNbO_3$. Charge density maps serve as a complementary tool for achieving a proper understanding of the electronic structure of the system being studied. In figure 4, atoms K, Nb and O are at

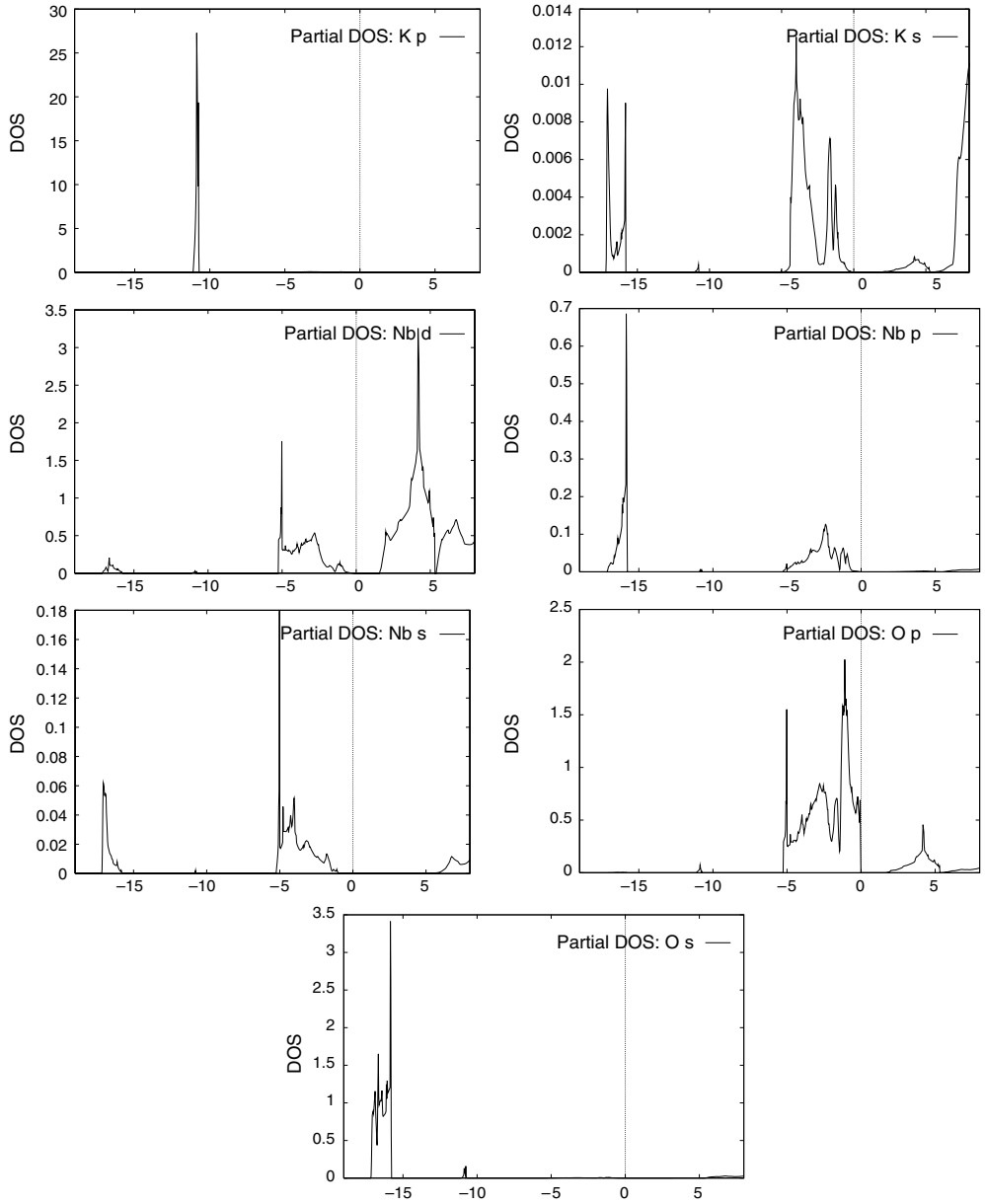

Figure 3. Site and angular momentum decomposed DOS for $KNbO_3$.

points (50, 0), (50, 50) and (25, 50) respectively as well as at (75, 50). In the figure, we see that there is interaction of charges between Nb and O due to Nb 4d and O 2p hybridization, thus showing that there is covalent bonding between niobium and oxygen. The near spherical charge distribution around the potassium site is negligible and as a result the potassium atom is fairly isolated which could indicate that the bonding between potassium and NbO_3 is mainly ionic. We therefore find that in cubic $KNbO_3$, there is bonding anisotropy. Our results are consistent with those of [18] for $KNbO_3$ and $KTaO_3$, of Wang [26] for $NaTaO_3$ and of Cohen and co-workers [64] for $BiTiO_3$.

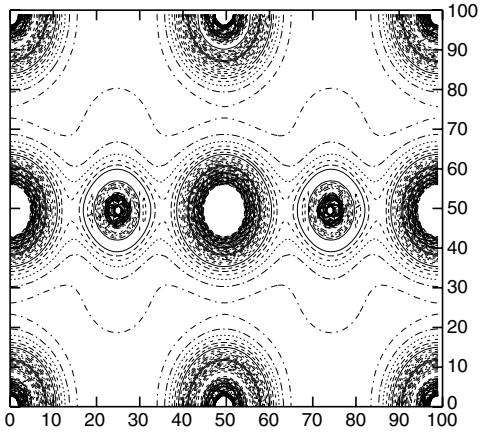

Figure 4. Valence charge density plots for cubic $KNbO_3$ in the (110) plane.

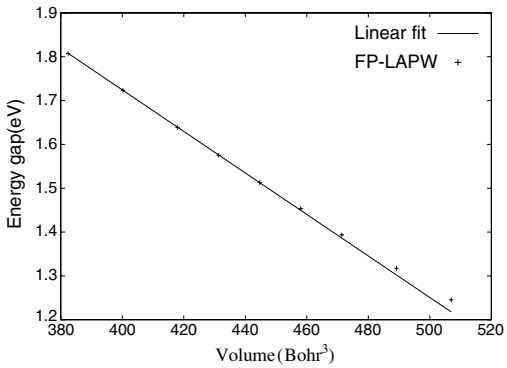

Figure 5. The calculated volume dependence of the indirect (R $\rightarrow$ Γ) energy gap of $KNbO_3$ (crosses). The solid line represents a linear fit to the theoretical results.

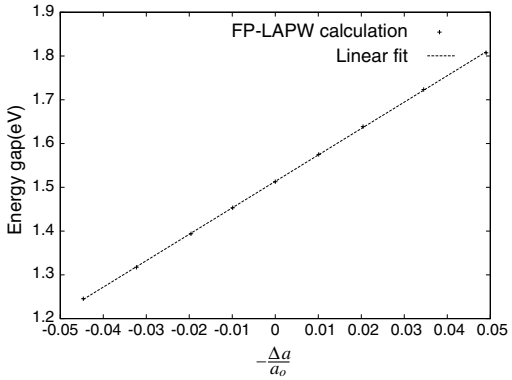

Figure 6. The theoretical dependence of the indirect (R $\rightarrow$ Γ) band gap of $KNbO_3$ as a function of the relative variation of the lattice constant.

In figure 5, the volume dependence of the energy gap of $KNbO_3$ is displayed. The calculations were performed using the FP-LAPW method within the GGA by applying

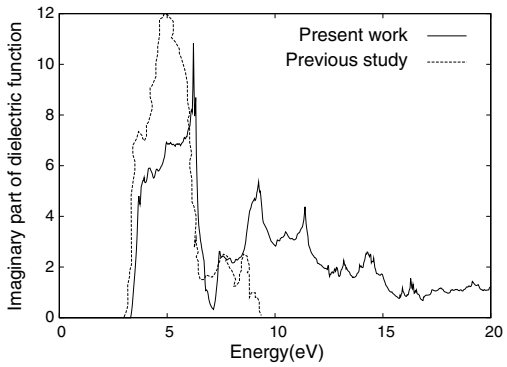

Figure 7. The calculated imaginary part of the dielectric function of cubic $KNbO_3$. The dashed curve shows the theoretical results of Castet-Mejean and Michel-Calendini [33] for $KNbO_3$ in the orthorhombic phase.

equation (3). It is seen that the energy gap increases with volume and is almost linearly dependent on volume with a slope of $(\partial E_g/\partial V) = -0.004\,74$ for lattice constants below the equilibrium volume ($V_0 = 444.69$ Bohr^3). For lattice constants higher than a_0, the volume dependence deviates from being linear. The pressure coefficient given in equation (3) is determined from the linear region of the energy gap versus volume plot [45, 46]. Our calculations yield a pressure coefficient, $(\partial E_g^{(R\to\Gamma)}/\partial P)$, of 12.3 meV GPa^{-1}. This band gap pressure behaviour is in agreement with previous studies [59]. The increase in band gap with decrease in volume appears to arise from the faster increase in the energy of the conduction band minimum than the valence band maximum under pressure. We also account for the volume deformation potential ($a_V^{(R\to\Gamma)}$) using the expression [65, 66]:

$$a_V^{(R\to\Gamma)} = \frac{dE_g^{(R\to\Gamma)}}{d\ln V} = -B\frac{dE_g^{(R\to\Gamma)}}{dp}, \tag{14}$$

where B is the bulk modulus. This yields $a_V^{(R\to\Gamma)} = -2.10$ eV.

The calculated dependence of the band gap on the relative variation in the lattice constant is displayed in figure 6. The variation shows a linear behaviour when represented through the equation

$$E_0^{R-\Gamma}(a) = A + B\left(\frac{-\Delta a}{a_0}\right) \tag{15}$$

where $\Delta a = a - a_0$ is change in lattice constant and a_0 is the equilibrium lattice constant at zero pressure. From the linear fit, the values of A and B were found to be 1.514 and 6.039 eV respectively. This predicted linear relation is in agreement with the result of Zhu *et al* [67] but in contrast to the sublinear or supralinear behaviour seen in most semiconducting compounds [68, 69].

3.3. Optical properties

In this section, we examine the optical response functions. The imaginary (ε_2) and the real (ε_1) parts of the dielectric function were calculated using equations (5) and (6) as well as the DFT scissors-operator approximation (equation (13)). The calculated spectra are displayed in figures 7 and 8. The shifted spectrum (solid curve) is compared to that from a previous theoretical study (dashed curve) taken from [33]. It is observed that the theoretical peak at

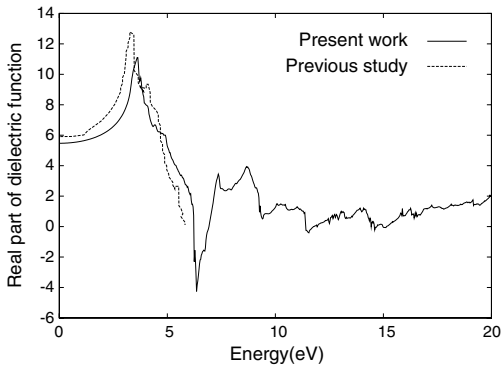

Figure 8. The calculated real part of the dielectric function of $KNbO_3$. The dashed curve shows the theoretical results of Castet-Mejean and Michel-Calendini [33] for $KNbO_3$ in the orthorhombic phase.

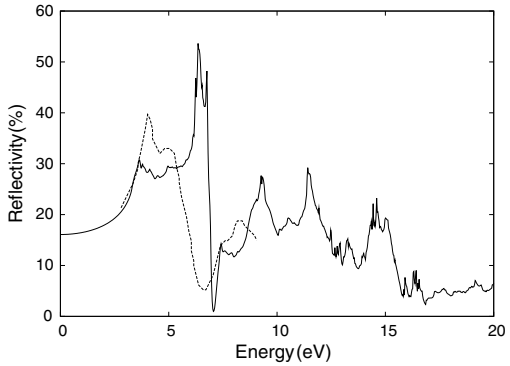

Figure 9. Reflectivity spectra for $KNbO_3$. The continuous curve shows the theoretical calculation; the dashed curve shows the measured spectra [31] for $KNbO_3$ in the orthorhombic phase.

6.22 eV is lower in amplitude than the experimental one. This could be interpreted as being probably due to the neglect of excitonic and local field effects [70] or lifetime broadening [71].

In order to account for the structures observed in the optical spectra, it is customary to consider transitions from occupied to unoccupied bands in the electronic energy band structure especially at high symmetry points in the Brillouin zone. For the absorptive part of the dielectric function ε_2, shown in figure 7, the highest peak in ε_2 at ∼6.22 eV arises from O 2p → Nb 4d t_{2g} at the R point. This is followed by other smaller peaks at about 9.3 and 11.4 eV with that at 9.3 eV exhibiting slightly higher amplitude. The positions of these peaks are in fair agreement with the results of [33] for the orthorhombic phase also displayed in the figure with a dashed curve. The minimum in ε_2 occurs at 7.14 eV.

In the dispersive part, ε_1, of the dielectric function shown in figure 8, the calculated spectra have been obtained by Kramers–Kronig transformation of the shifted ε_2 spectra. The first peak in ε_1 at about 3.6 eV originates from O 2p → Nb 4d t_{2g} at probably the Γ point or the X points. This peak is followed by a decrease which reaches a global minimum (between 0 and 20 eV) at 6.3 eV, and fairly small peaks at 7.4 and 8.7 eV. Our results are compared with the calculations of Castet-Mejean and Michel-Calendini [33] displayed with crosses.

The reflectivity spectra are shown in figure 9. The calculated reflectivity is shown with a solid curve, while the crosses show the measured results [31]. The spectra exhibit peaks

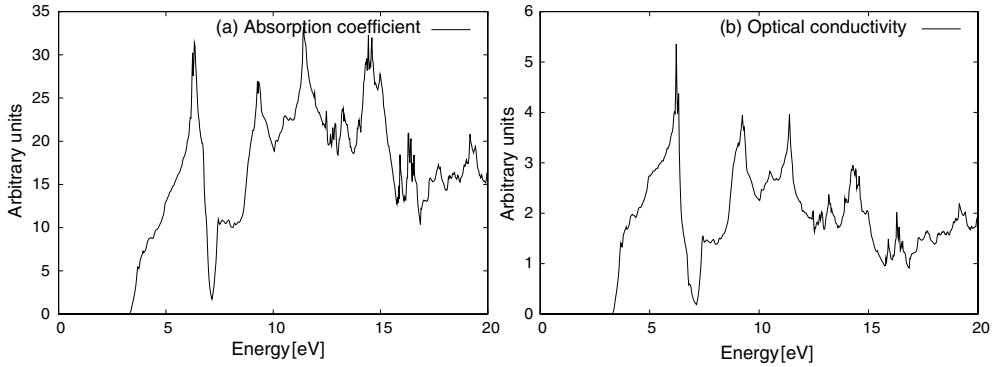

Figure 10. The calculated (a) absorption coefficient and (b) real part of the optical conductivity of $KNbO_3$ in the cubic phase.

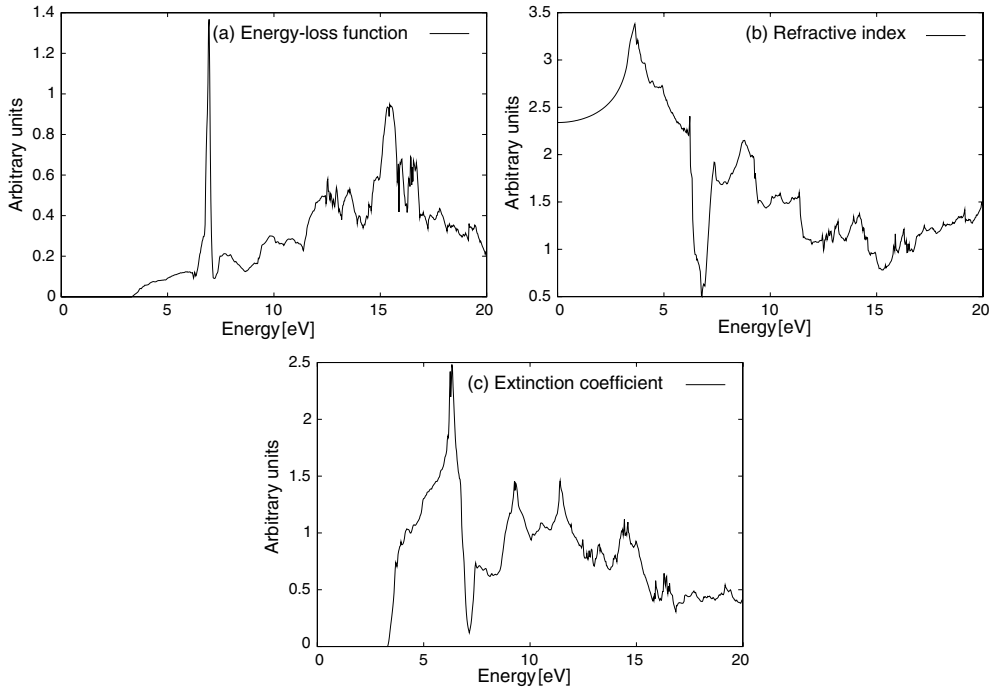

Figure 11. The theoretical (a) electron energy-loss spectrum, (b) refractive index and (c) extinction coefficient of cubic $KNbO_3$.

similar to those in the dielectric function. We find also that the reflectivity varies widely as a function of energy. This could possibly make the compound $KNbO_3$ suitable for a variety of optical applications. It is important to note that the discrepancy between the theoretically calculated reflectivity spectra and the experimental result [31] is perhaps due to the fact that the measured reflectivity is for orthorhombic $KNbO_3$. The deviations may therefore reflect the strong changes in the Nb 4d derived conduction band produced by the displacement of atoms from their perovskite structure positions.

The calculated linear absorption spectrum and the real part of the optical conductivity are displayed in figure 10. The fundamental absorption edge starts from about 3.3 eV which

corresponds to the direct Γ–Γ transition. This originates from the transition from the O 2p electron states located at the top of the valence band to the empty Nb 4d electron states dominating the bottom of the conduction bands. The first peak in the absorption spectrum occurs at 6.3 eV. Other peaks occur at 9.3, 11.5 and 14.5 eV. Similar structures are seen in the recent calculations of Duan *et al* [37] on the orthorhombic phase of $KNbO_3$. Also in figure 10(b), the energy dependence of the real part of the optical conductivity is displayed. The origin of the structures in the imaginary part of the dielectric function also explains the structures in the optical conductivity. In addition, the amplitude of the structures in the optical conductivity goes as $\omega\varepsilon_2$.

The electron energy-loss function $-\operatorname{Im}(\varepsilon)^{-1}$ of $KNbO_3$ was calculated from the $\operatorname{Im}(\varepsilon)$. This is displayed in figure 11(a). This function is usually large at the plasmon energy whose position corresponds to $\epsilon_1(\omega) = 0$, provided that $\epsilon_2(\omega)$ is reasonably smooth in these regions [72], thus giving the plasmon energy as ∼7.0 eV. The other peaks arise at the energies of the interband transitions from the valence bands to the lower and upper conduction bands. Also in the figure (figures 11(b) and (c)) are displayed the refractive index and extinction coefficient. In the far infrared region, the refractive index is about 2.3 and it increases with energy in the transparency region reaching a peak in the ultraviolet at about 3.6 eV due to probably interband transitions. It then decreases to a minimum level at 6.9 eV. On the other hand, the peak in the extinction coefficient occurs at 6.2 eV.

Generally, we have performed the calculations over a wide energy range leading to very high energy transitions such that contributions originating from each of the atoms will be accommodated. It is to be noted that there are no experimental results for the optical properties for the paraelectric cubic phase of $KNbO_3$. We expect that our theoretical studies will motivate experimental work aimed at investigating the optical properties of the cubic phase of this compound.

4. Conclusions

A full-potential investigation of the electronic structure, chemical bonding and optical properties of $KNbO_3$ in the paraelectric cubic phase has been performed using the linearized augmented plane wave method. The results yield band structures that are in agreement with previous theoretical studies. The calculations show that the band gap is indirect ($R \rightarrow \Gamma$). Our calculated fundamental gap is 1.58 eV and increases with increase in pressure. The total DOS obtained from our full-potential calculations are discussed. It is found that there is significant hybridization between Nb d and O p states in the compound. Analysis of the nature of the chemical bonding indicates that the interaction between Nb and O is covalent and that the one between K and NbO_3 is ionic. The optical properties such as the dielectric function, reflectivity, absorption coefficient, real part of the optical conductivity, electron energy-loss function, refractive index and extinction coefficient have been studied. Using the band structure, we have analysed the interband contribution to the optical response functions. It is found that the origin of the peaks in the dielectric function probably also explains the structures in the spectra of these optical functions.

Acknowledgments

The author would like to thank the International Atomic Energy Agency and UNESCO for hospitality at the Abdus Salam International Centre for Theoretical Physics (ICTP), Trieste, Italy, where this work was started. Financial support from the Swedish International

Development Cooperation Agency (SIDA) during my visit to ICTP as a regular associate is acknowledged. My thanks also go to Professor P Blaha, K Schwarz and J L Luitz for providing the program.

References

[1] Postnikov A V *et al* 1998 *Ferroelectrics* **206/207** 69
[2] Xu Y-N, Ching W Y and French R H 1990 *Ferroelectrics* **111** 23
[3] Singh D J and Boyer L L 1992 *Ferroelectrics* **136** 95
[4] Lines M E and Glass A M 1977 *Principles and Applications of Ferroelectrics and Related Materials* (Oxford: Clarendon) and references therein
[5] Rici Y and Krakauer H 1995 *Phys. Rev. Lett.* **74** 4067
[6] Gunter P 1982 *Phys. Rep.* **93** 199
[7] Vanderbilt D 1997 *Curr. Opin. Solid State Mater. Sci.* **2** 701
[8] Fluckiger U and Arend H 1987 *J. Cryst. Growth* **43** 406
[9] Donafeng X and Zhang S 1997 *J. Phys. Chem. Solids* **58** 1399
[10] Edwardson P J 1989 *Phys. Rev. Lett.* **63** 55
[11] Postnikov A V, Neumann T, Borstel G and Methfessel M 1993 *Phys. Rev.* B **48** 5910
[12] King-Smith R D and Vanderbilt D 1994 *Phys. Rev.* B **49** 5828
[13] Zhong W, King-Smith R D and Vanderbilt D 1995 *Phys. Rev. Lett.* **74** 4067
[14] Eglitis R I, Postnikov A V and Borstel G 1996 *Phys. Rev.* B **54** 2421
[15] Singh D J 1995 *Phys. Rev.* B **52** 12559
[16] Resta R, Posternak M and Baldereschi A 1993 *Phys. Rev. Lett.* **70** 1010
[17] Wang Y X, Zhong W L, Wang C L and Zhang P L 2001 *Phys. Rev. Lett.* A **291** 338
[18] Neumann T, Borstel G, Scharfschwerdt C and Neumann M 1992 *Phys. Rev.* B **46** 10623
[19] Xu Y-N, Ching W Y and French R H 1990 *Ferroelectrics* **111** 23
[20] Delin A, Eriksson A O, Ahuja R, Johansson B, Brooks M S S, Gasche T, Auluck S and Wills J M 1996 *Phys. Rev.* B **54** 1673
[21] Saha S, Sinha T P and Mookerjee A 2000 *Phys. Rev.* B **62** 8828
[22] Saha S, Sinha T P and Mookerjee A 2000 *J. Phys.: Condens. Matter* **12** 3325
[23] Saha S, Sinha T P and Mookerjee A 2000 *Eur. Phys. J.* B **18** 207
[24] Wang Y X, Zhong W L, Wang C L and Zhang P L 2001 *Solid State Commun.* **120** 133
[25] Wang Y X, Zhong W L, Wang C L and Zhang P L 2001 *Phys. Lett.* A **120** 133
[26] Wang Y X, Zhong W L, Wang C L and Zhang P L 2001 *Solid State Commun.* **120** 137
[27] Ravindran P, Delin A, Johansson B and Eriksson O 1999 *Phys. Rev.* B **59** 1776
[28] Wang Y X, Zhong W L, Wang C L, Zhang P L and Peng Y P 2001 *Phys. Lett.* A **269** 252
[29] Cardona M 1965 *Phys. Rev.* A **140** 651
[30] Kurtz S K 1966 *Proc. Int. Mtg on Ferroelectricity (Prague)* **1** 419
[31] Wiesendanger E and Guntherodt G 1974 *Solid State Commun.* **14** 303
[32] Michel-Calendini F M and Castet-Mejean L 1976 *Ferroelectrics* **13** 367
[33] Castet-Mejean L and Michel-Calendini F M 1978 *J. Phys. C: Solid State Phys.* **11** 2195
[34] Michel-Calendini F M, Chermette H and Weber J 1980 *J. Phys. C: Solid State Phys.* **13** 1427
[35] Castet-Mejean L 1986 *J. Phys. C: Solid State Phys.* **19** 1637
[36] Krasovskii E E, Krasovska O V and Schattke W 1997 *J. Electron Spectrosc. Relat. Phenom.* **83** 121
[37] Duan C-G, Mei W N, Liu J and Hardy J R 2001 *J. Phys.: Condens. Matter* **13** 8189
[38] Singh D J 1994 *Planewaves, Pseudopotentials and the LAPW Method* (Boston, MA: Kluwer–Academic)
[39] Perdew J P, Burke S and Ernzerhof M 1996 *Phys. Rev. Lett.* **77** 3865
Perdew J P, Burke S and Ernzerhof M 1997 *Phys. Rev. Lett.* **78** 1396 (erratum)
[40] Hellwege K-H (ed) 1981 Ferroelectrics and related substances *Numerical Data and Functional Relationships in Science and Technology* (*Landolt–Börnstein New Series* Group III, vol 16a) (Berlin: Springer)
[41] Shirane G, Newnham R and Pepinsky R 1954 *Phys. Rev.* **96** 581
[42] Blaha P, Schwarz K and Luitz J 1997 *WIEN97, a Full Potential Linearized Augmented Plane Wave Package for Calculating Crystal Properties* Technical University of Vienna (ISBN 3-9501031-0-4)
This is an improved and updated Unix version of the original copyrighted WIEN-code, which was published by Blaha P, Schwarz K, Sorantin P and Trickey S B 1990 *Comput. Phys. Commun.* **59** 399
[43] Hohenberg P and Kohn W 1964 *Phys. Rev.* **136** 864
[44] Kohn W and Sham L J 1965 *Phys. Rev.* A **140** 1133
[45] Lach-hab M, Keegan M, Papaconstantopoulos D A and Mehl M J 2000 *J. Phys. Chem. Solids* **61** 1639

[46] Lach-hab M, Papaconstantopoulos D A and Mehl M J 2002 *J. Phys. Chem. Solids* **63** 833
[47] Ambrosch-Draxl C and Abt R 1998 The calculation of optical properties within WIEN97 *ICTP Lecture Notes* unpublished
[48] Yu Y P and Cardona M 1999 *Fundamentals of Semiconductors: Physics and Materials Properties* 2nd edn (Berlin: Springer) p 241
[49] Fox M 2001 *Optical Properties of Solids* (New York: Oxford University Press) p 6
[50] Delin A, Eriksson A O, Ahuja R, Johansson B, Brooks M S S, Gasche T, Auluck S and Wills J M 1996 *Phys. Rev.* B **54** 1673
[51] Pickett W E 1986 *Comment. Solid State Phys.* **12** 57
[52] Hybertsen M S and Louie S G 1986 *Phys. Rev.* B **34** 5390
[53] Levine Z H and Allan D C 1991 *Phys. Rev.* B **43** 4187
[54] Del Sole R and Girlanda R 1993 *Phys. Rev.* B **48** 11789
[55] Persson C, Ahuja R, Ferreira da Silva A and Johansson B 2001 *J. Phys.: Condens. Matter* **13** 8945
[56] Stahrenberg K, Herrmann Th, Wilmers K, Esser N, Richter W and Lee M J G 2001 *Phys. Rev.* B **64** 115111
[57] Abraham Y, Holzwarth N A W and Williams R T 2000 *Phys. Rev.* B **62** 1733
[58] Murnaghan F D 1994 *Proc. Natl Acad. Sci. USA* **30** 244
[59] Singh D J 1995 *Ferroelectrics* **164** 143
[60] Wiesendanger E 1974 *Ferroelectrics* **6** 203
[61] Singh D J 1996 *Phys. Rev.* B **53** 176
[62] Mattheiss L F 1972 *Phys. Rev.* B **6** 4718
[63] Godby R W, Schluther M and Sham L J 1987 *Phys. Rev.* B **36** 6497
[64] Cohen R E and Krakauer H 1990 *Phys. Rev.* B **48** 6416
Cohen R E 1992 *Nature* **358** 136
[65] Wei S and Zunger A 1999 *Phys. Rev.* B **60** 5404
[66] Dridi Z, Bouhafs B and Ruterana P 2002 *New J. Phys.* **4** 1.1–1.15
[67] Zhu X, Fay S and Louie S G 1989 *Phys. Rev.* B **39** 7840
[68] Ves S, Strossner K, Christensen M E, Kim K M and Cardona M 1985 *Solid State Commun.* **56** 479
[69] Rodriguez C O, Peltzer y Blanca E L and Cappannini O M 1986 *Phys. Rev.* B **33** 8436
[70] Hanke W and Sham L J 1980 *Phys. Rev.* B **21** 4656
[71] Delin A, Ravindran P, Eriksson O and Wills J M 1998 *Int. J. Quantum. Chem.* **69** 349
[72] Wang C S and Klein B M 1981 *Phys. Rev.* B **24** 3417